Nanoscale

Anharmonicity-induced thermal rectification of a single diblock molecular junction inspired by the Aviram–Ratner diode

Journal:	*Nanoscale*
Manuscript ID	NR-ART-11-2024-004716.R1
Article Type:	Paper
Date Submitted by the Author:	12-Feb-2025
Complete List of Authors:	Nakamura, Hisao; National Institute of Advanced Industrial Science and Technology Tsukuba Center Tsukuba Central, Karasawa, Naoyuki; Saitama University

Anharmonicity-induced thermal rectification of a single diblock molecular junction inspired by the Aviram–Ratner diode

Hisao Nakamura and Naoyuki Karasawa*

National Institute of Advanced Industrial Science and Technology (AIST),

Tsukuba Central 2, 1-1-1 Umezono, Tsukuba, Ibaraki 305-8568, Japan

* hs-nakamura@aist.go.jp

ABSTRACT

We examined the design of a unimolecular thermal diode inspired by the concept of the Aviram–Ratner diode and analyzed the anharmonic effects of molecular vibrations in the junction on heat transport. Our central idea involves (i) reconfiguring the electron donor and acceptor into "phonon scatter-rich" (strong anharmonicity) and "phonon scatter-deficient" (weak anharmonicity) moieties and (ii) using hydrogen bonds as thermal spacers to prevent nonlocal anharmonic effects on the thermal transport channel. To evaluate the effects of anharmonic interactions, we developed a fictitious electrode model combined with nonequilibrium Green's function theory and then performed thermal transport calculations. Our results indicate that hydrogen bonds are very promising for constructing thermal molecular device materials. Reducing the thermal gradient and mitigating inelastic phonon scattering effects at the interface are critical for increasing the rectification ratio in single molecular junctions.

Introduction

There has been substantial progress in the investigation of electric transport in molecular junctions, advancing toward applications in minimal and functional devices, such as nonvolatile memory[1], spintronics[2], single-electron transistors[3], and thermoelectric materials[4]. Understanding heat transport through the junction is key for controlling Joule heating[5] or improving energy conversion efficiency[6], among other relevant phenomena of functional molecular devices[7].

Besides applications in functional devices, studies of molecular devices often provide useful insights into understanding the operating mechanism of solid-state nanodevices and designing device materials[8]. The heat transport of a single molecular junction encompasses a wealth of unresolved fundamental problems, such as the nonequilibrium quantum transport[9], energy exchange[10], and dissipation processes[11] at the nanoscale. Hereafter, we use the term "thermal transport (conductance)" to represent the phononic part of heat transport simply because the electric heat transport is much smaller in our systems of focus.

Recently, several groups have reported thermal conductance measurements of molecular self-assembled monolayers[12] and single molecular junctions[13,14] using thermoreflectance and break junction techniques with embedded thermal probes or heat flux sensors, respectively. More recently, scanning thermal microscopy has been used to visualize the thermal transport[15]. Moreover, the thermal transport process has been analyzed theoretically using molecular dynamics (MD)[16], the Boltzmann transport equation[17], and the nonequilibrium Green's function (NEGF) method[18, 19]. The latter is based on quantum transport theory, and substantial progress has been made in its application to electric and thermal transport in molecular junctions. According to recent experimental and theoretical studies, characteristic thermal transport phenomena at the nanoscale, such as phonon localization[20], the transition from ballistic to hopping transport[21], interference[22], resonance[23], and rectification[24], have been suggested. Interestingly, very similar properties have been found in molecular electronics research[6], implying that some of the concepts used in design of molecular electronics may inspire the design of thermal properties based on chemical properties, such as chemical bonding[25].

Based on this consideration, we focus on thermal rectification of a molecular device realized by an intrinsic property of a bridge molecule. Aviram and Ratner proposed the theoretical concept of a molecular (electric) diode[26], which remains a cornerstone when studying molecular device functionality. The Aviram–Ratner (AR) diode molecule consists of $\pi-\text{donor}$ (D) and $\pi-$ acceptor (A) molecules separated by a σ bond spacer, commonly denoted as $D-\sigma-A$. The D and A components are analogous to *p*-type (*n*-type) semiconductors in a bulk *pn* junction. Although the

forward direction of the AR diode is generally expected to match that of bulk *pn* rectification, this is not always the case[27]. To simplify the AR diode and provide a template for analyzing its rectification mechanism, a diblock molecule resembling a *pn* junction was synthesized controlling its molecular orientation relative to the electrodes. Clear rectification of this AR or *pn*-resembling diblock molecule was demonstrated by comparing with a symmetric diblock molecule, where the forward direction aligns with that of the *pn* junction[28]. We aim to extend the concept of the diblock molecular diode, referred to as "AR-resembling," to design an "unimolecular" thermal diode via NEGF calculations. Our central idea for constructing the AR-resembling thermal diode involves two key components. First, we reinterpret D and A, which respond to a bias voltage (electric field), to respond to a temperature gradient, and changed the carrier from electrons to phonons. Ma and Tian used MD to demonstrate thermal rectification in asymmetric polymer molecule, which consisted of polynorbornene (PNb) and polystyrene[29]. The former acted as a thermal conductor frame. The PNb units were asymmetrically modified by polystyrene brushes. We adapted this approach to a single-molecule level by modeling D and A as blocks with "phonon scatter-rich" (strong anharmonicity) and "phonon scatter-deficient" (weak anharmonicity) properties. Second, we employed hydrogen bonds (HB) as thermal spacers to prevent nonlocal anharmonic effects on the thermal transport channel. To incorporate anharmonic effects, we developed a practical scheme to model the anharmonic self-energy term and determine the necessary parameters for NEGF calculations of a molecular junction.

Theoretical method

The NEGF method is promising for analyzing thermal transport in single molecular junctions and solid heterojunction systems. Based on perturbation theory, the NEGF formulation can be extended to evaluate the self-energy term of phonon–phonon scattering processes[19, 30]. However, this approach requires large computational resources[31] and thus challenging for complex molecular junctions. As an alternative practical approach, we adopted the fictitious electrode method[32, 33]. In this model, the disruption of phase coherence and energy exchange of the heat current due to anharmonic effects are evaluated through in- and out-flux via each fictitious electrode in thermal equilibrium, functioning as thermal baths[34]. The self-energy terms of the anharmonic effect, $\Pi_{\mathrm{vib}}^{r,a,<,>}$, are defined from the atomic degrees of freedom (DoF) $\vec{x}_{I_a} = (x_\mu)$, where I_a is the atom index and a represents its atomic species. Recently, we developed a single fictitious electrode model similar to that developed by Datta[33], where the phonon Green's function of the target molecular junction was included in the self-energy[35]. The retarded/advanced self-energy terms of the anharmonic effect are functions of both the energy ω and local temperature T_μ of each DoF as follows:

$$\Pi_{\mathrm{vib},\mu\mu}^{r}(\omega,T_\mu) = \frac{-i\omega}{\tau_a(\omega,T_\mu)} g_\mu(\omega). \quad (1)$$

The term $\tau_a(\omega,T)$ is the relaxation time function of the atomic species a related to atom I_a. $\tau_a(\omega,T)$ is evaluated without empirical parameters, as explained later. The function $g_\mu(\omega)$ is the correction term explicitly incorporating the phonon Green's function into the fictitious electrode model. It is expressed using the retarded and advanced phonon Green's functions D^r and D^a of the molecular junction:

$$g_\mu(\omega) = \left(\frac{i}{\pi}\right)\Omega_D \omega \overrightarrow{u_\mu} \mathrm{Diag}[D^r - D^a]\overrightarrow{u_\mu}^t, \qquad (2)$$

where the vector $\overrightarrow{u_\mu}$ represents the normalized coupling strength with the fictitious electrode, and $\overrightarrow{u_\mu}^t$ is its transpose. Ω_D is the normalization factor that ensures the average of g_μ over the focused energy region is 1. The function $g_\mu(\omega)$ accounts for the number of accessible states for energy redistribution of each phonon due to anharmonicity. The lesser self-energy is then written as follows:

$$\Pi^{<}_{\mathrm{vib},\mu\mu}(\omega,T_\mu,T_{fc}) = f_{BE}(\omega,T_{fc})(\Pi^{r}_{\mathrm{vib},\mu\mu} - \Pi^{a}_{\mathrm{vib},\mu\mu}), \quad (3)$$

where f_{BE} is the Bose-Einstein function, and T_{fc} is the temperature of the fictitious electrode, which satisfies the conservation of heat flux. Practically, T_{fc} is the temperature that minimizes the net flux at the fictitious electrode. When the temperatures of the left and right thermalized electrodes are given as T_L and T_R, respectively, the heat current J_Q is expressed as follows:

$$J_Q = \int d\omega \frac{\hbar\omega}{2\pi}\mathrm{Tr}[\Gamma_L D^r \Gamma_R D^a](f_{BE}(\omega,T_L) - f_{BE}(\omega,T_R)) + \int d\omega \frac{\hbar\omega}{2\pi} Tr[\Gamma_L D^r \Gamma_{\mathrm{vib}} D^a](f_{BE}(\omega,T_L) - f_{BE}(\omega,T_{fc}))$$

$$= \int d\omega \frac{\hbar\omega}{2\pi}\mathcal{T}^{ela}(\omega)(f_{BE}(\omega,T_L) - f_{BE}(\omega,T_R)) + \int d\omega \frac{\hbar\omega}{2\pi}\mathcal{T}^{inel}(\omega)(f_{BE}(\omega,T_L) - f_{BE}(\omega,T_{fc})) \quad (4)$$

The term Γ_α is defined as $(\Pi^r_\alpha - \Pi^r_\alpha)$, where $\Pi^{r/a}_\alpha$ represents the retarded/advanced self-energy of the left ($\alpha = L$), right ($\alpha = R$), and fictitious ($\alpha = \mathrm{vib}$) electrodes, respectively. The first term in Eq. (4) is called the elastic term, which consists of the sum of a ballistic term and a correction term due to the elastic scatterings of phonons. The second term represents the incoherent or inelastic scattering effects. We refer $\mathcal{T}^{ela}(\omega)$ and $\mathcal{T}^{inel}(\omega)$ as elastic and inelastic transmission coefficient, respectively. If the difference between T_L and T_R is sufficiently small, the thermal conductance, κ_{ph}, is evaluated as follows:

$$\kappa_{ph}\left(T \sim \frac{T_L+T_R}{2}\right) = \frac{J_Q}{T_L - T_R}. \qquad (5)$$

The remaining challenge is parameterizing the relaxation function $\tau_a(\omega,T)$. As outlined in Refs. [36], anharmonic interactions in the equation of motion can be treated as the stochastic term of the Langevin equation. This model of the stochastic term is equivalent to introducing a fictitious electrode to the harmonic phonon Green's function:

$$M_\mu \frac{d^2 x_\mu}{dt^2} = -\frac{1}{2}\sum_{\boldsymbol{\nu}} K_{\boldsymbol{\mu\nu}} x_\nu - M_\mu \int_0^t ds \Gamma_\mu(s) \frac{dx_\mu(t-s)}{dt} + \xi_\mu(t). \quad (6)$$

Here, K, Γ, and ξ are the harmonic constant matrix, friction tensor, and random force, respectively. The friction constant in frequency space is then given as $\tau^{-1}_{\mu\in I_a}(\omega,T) = \Gamma_\mu(\omega,T)$. Assuming that (i) each term depends only on the atomic species and (ii) the relaxation time can be expressed by the separation of a characteristic time constant (or friction constant) and a part from a colored noise, we can rewrite the friction term as follows:

$$\tau^{-1}_{\mu\in I_a}(\omega,T) \cong \tau_a^{-1}(\omega,T) \cong \tau_{0a}^{-1} f_a(\omega,T) = \Gamma_{0a} f_a(\omega,T). \quad (7)$$

Suppose we have a data set of MD trajectories for the molecular junction system $\left(x_\mu(t), \frac{dx_\mu}{dt}\right)$, where the initial condition is set to satisfy the law of equipartition for each vibrational (normal) mode, $\frac{3}{2}k_B T$, i.e., thermally equilibrated oscillators. While there are several methods to extract color noise from these MD data[37], we took rough approximated procedure since our purpose is to parameterize the function by color noise relating to each atomic species. The protocol and adopted MD calculation are summarized in the Supplementary Information (SI).

Finally, we comment on the differences between the present and Büttiker probe (BP) models[32, 34]. In the standard BP model, each structureless thermal bath is independently connected to each atomic site, and thermal equilibrium is assumed between the thermal bath and the connected atom. The local temperature of each atom is defined by its equilibrium temperature, which means the local temperature used to determine the vibrational relaxation time is not related directly to the energy of atomic motion. In contrast, our model adopts a thermal bath represented by the retarded Green's function of the target molecular junction just as the case of electron-phonon interaction by Datta's approach[38]. Therefore, heat dissipation path to the thermal bath depends on phonon density of states (DOS) of the junction. Additionally, the local temperature T_μ in the term $\tau_a^{-1}\left(\omega, T = T_\mu\right)$ is defined by the kinetic energy of each atom. This is consistent with the definition of $\tau_a^{-1}(\omega,T)$ in our model. The following calculations of thermal transport properties of the diblock molecular junctions were performed using our in-house code[39], interfaced with the Smeagol program package[40].

Thermal rectification of diblock molecule

We begin our discussion with the phonon thermal conductance of diblock molecular junctions. We consider a diblock molecule consisting of two block molecules (fragments) bridged by a spacer through which heat current flows. Here, we adopted two types of chemical bonds as spacers: a hydrogen bond (weak chemical bond) and a covalent bond (triple bond). Phenyl and pyridine were used as blocking molecules to minimize asymmetric effects derived from the asymmetric contact structure. We thus examined three kinds of diblock molecules, denoted as C_2Ph_2, CHO_2PhPy, and

$(CHO_2)_2Ph_2$, Figure 1. Each diblock molecule is connected to the 3×3 Au(111) electrodes by thiol anchors; the left and right electrodes consisted of six and five atomic layers, respectively. Atomic positions were determined by relaxing all atoms, and the adsorption site of the thiol anchor was the bridge site for all systems.

The anharmonic self-energy term was expressed using a model function based on preliminary MD simulations, as described above. We evaluated the numerical values of $\tau_a^{-1}(\omega,T)$ as a function of ω for C, H, O, N, and S atomic species, with temperatures set to 200, 250, 300, 400, and 600 K, respectively. For convenience in NEGF calculations and to ensure the transferability of the model, we represented the obtained colored noise using activation functions,

$$f_a(\omega,T) = A\sinh(\alpha_T T) + B\tanh(\beta_T T)\sinh(\alpha_\omega \omega), \quad (8)$$

where A, α_T, β_T, and α_ω are fitting parameters determined for each atomic species a. The flow of calculations is provided in the SI. The set of fitted parameters for the CHO_2PhPy junction is presented in Table 1. It is worth noting that the couplings of internal molecular vibrations and rattling modes through phonons of the electrodes should be considered to model the anharmonic effects of a single molecular junction. We used the same parameter set to calculate the anharmonic self-energy of the other junctions. We note that the introduced function in Eq. (8) is an ad hoc model function, not universal scaling function, though it reproduces the calculated spectra well and satisfies the condition that the f_a become zero when the temperature equals zero, i.e., thermal transport becomes ballistic at low temperature limit. In molecular junctions including metallic electrodes, normal mode frequencies are much higher than those of electrodes. The above activation functions will be flexible to express frequency of atomic motions coupled with phonon of electrodes, which is far from molecular normal mode frequency. On the other hands, it may not be suitable to represent molecular crystal systems, where thermal conducting frequency is close to that of molecular normal mode. In such case, Debye model or Callaway model function[41] may be more suitable.

Figure 2 (a), (b), and (c) show the results of thermal conductance $\kappa_{ph}(T)$ for the C_2Ph_2, CHO_2PhPy, and $(CHO_2)_2Ph_2$ junctions, respectively. We also calculated the thermal conductance using the ballistic approximation for comparison. In all cases, the error of the results by the ballistic approximation was typically within only 2 % at temperatures lower than room temperature. Furthermore, the HB was a thermal conductor comparable to the covalent bond, despite the large difference in bond strength. It is known that molecular rattling modes and low-frequency modes of molecular vibration are crucial in the thermal transport of molecular junctions due to phonon mismatching between the molecule and the electrodes. In the case of C_2Ph_2, the two phenyl blocks are integrated via a rigid triple bond, making Ph_2 the rattling moiety. In contrast, the HB spacer separates the two moieties for CHO_2PhPy and $(CHO_2)_2Ph_2$ well. Thus, these molecules have two rattling moieties, consisting of the independent

rattling motion of each phenyl or pyridine. As a result, the HB spacer is a thermal conductor comparable to the covalent bond. Above 400 K, we observed that κ_{ph}(T) clearly decreases with increasing temperature T, a behavior often seen with elastic phonon–phonon scattering or dephasing effects, though the rate of decrease was smaller than for standard inorganic crystals or homogeneous nanowires (approximately $T^{-1.0}$). The rate of decrease for κ_{ph}(T) was $T^{-0.02}$ for C_2Ph_2 and CHO_2PhPy, and $T^{-0.05}$ for the $(CHO_2)_2Ph_2$ junction. The larger dephasing effect observed for $(CHO_2)_2Ph_2$ compared to C_2Ph_2 and CHO_2PhPy indicates that the HB spacer acts as both a scatter of phonons and a heat conductor.

To further analyze the anharmonic effects, we calculated the cumulative thermal conductance $\kappa_{cum}(E)$ in the high-temperature regime (T = 500 K). The results are shown in Figure 3. Above 2.0 THz, which is close to the first peak position of the phonon density DOS of the Au electrode, substantial discrepancies from the ballistic approximation were found in all cases (Figure 3 (a), (b), and (c)). This is consistent with the understanding that anharmonic effects on molecular vibration and thermal transport are triggered through coupling with Au bulk/surface phonons. We also evaluated a portion of the inelastic scattering, represented by the blue dotted lines in Figure 3. The inelastic thermal current, given in the second term of Eq. 4, is positive, similar to the inelastic electric current due to the electron–phonon interaction. Although the increase in conductance due to the inelastic scattering effect was smaller than the decrease due to the dephasing effect of elastic scatterings in the single molecular junctions under study, our calculated results agree with the reported prediction[42], i.e., inelastic effects at the junction assist thermal transport. Dephasing effect to the phonon DOS and elastic transmission coefficient is given in SI for $(CHO_2)_2Ph_2$ as reference.

Before proceeding with further discussion of anharmonic effect on thermal transport, we comment to contribution of electric heat transport. Within the ballistic approximation to electric transport, electric thermal conductance $\kappa_e$is relating to electric conductance σ_e through the electric transmission coefficient. Typically, σ_e is lower than $10^{-3}G_0$ for single molecular junctions of organic molecules. In such case, the value of κ_e is close to order of 10^{-1} pW/K though κ_{ph} is often order of 10^{1} pW/K, i.e., electron contribution is negligible.[43] To validate the above argument, we calculated σ_e and κ_e of $(CHO_2)_2Ph_2$ junction at 300K (See SI) and fond that the value of κ_e were less than 0.01 time the value of κ_{ph}. Therefore, we omit electron contribution to thermal conductance in the below.

Now, we examine the possibility of an intrinsic “unimolecular” thermal diode by extending the concept of the AR diode. A study by Ma and Tian indicated that thermal rectification in a single polymer could be achieved by introducing side-chains asymmetrically as phonon scatterers[29]. We considered a diblock molecule consisting of phenyl (or pyridine) dressed with phonon scatterers and

pristine phenyl connected by an HB. Phonon scatterers can be achieved by inserting functional groups. We labeled the former as D^H and the latter as A^H, thus the diblock molecule is now an AR-resembling diblock molecule represented as D^H–(HB)–A^H. Since many phonon scatterers are on the D^H side, the dephasing effect due to anharmonicity is expected to be substantial when the D^H side is in the high-temperature regime. Therefore, the AR-resembling diblock molecule, D^H–(HB)–A^H, can be expected to function as a thermal diode, where the forward direction of thermal current is from A^H to D^H, analogous to conventional electric current (opposite to electron movement) in an AR diode or a *pn* junction built in a molecule.

To analyze the effects of asymmetric anharmonicity introduced by phonon scatterers (i.e., a simplified model of inserting functional groups for our purposes), we examined the correction of the self-energy term of the atomic site on the D^H side by changing the parameter Γ_{0a} for the calculation of the Green's function. Figure 1 shows the sites of enhanced anharmonicity and the labels of the AR-resembling diblock molecules. Bold letters correspond to the D^H moiety. For instance, CHO_2**Ph**Py indicates that the phenyl side is the D^H moiety. We selected the H atomic site connected to the C_1 atom, marked by a red circle in Figure 1, as the target to modify the self-energy term. The value Γ_{0a} of the target site was changed from Γ_{0H} to $5\Gamma_{0C} + 11\Gamma_{0H}$, as a rough model of the side-chain for phonon scatterer in Ph.

To clarify the analogy with the relationship between an electric diode and bias voltage, we introduced the reference temperature T_0 and the temperature difference ΔT defined as $\Delta T = T_A - T_D$. We denote the temperatures of the electrodes connected to A^H and D^H as T_A and T_D, respectively. When ΔT is set to a positive value, T_D is fixed at T_0 and T_A is verified. Conversely, when T_A is fixed at T_0, ΔT is set to a negative value. Thus, the positive temperature difference corresponds to the forward direction of rectification, and the rectification parameter η can be defined as follows:

$$\eta(\Delta T) = 1 - \frac{J_Q(\Delta T)}{J_Q(-\Delta T)} \quad . \qquad (10)$$

Table 2 summarizes the calculated results of η. We found that η increased as a function of ΔT for all the diblock molecules, with T_0 set at 100 K. The triple bond spacer, C_2**Ph**Ph, yielded the smallest rectification parameter compared to the single HB spacer, CHO_2**Ph**Py, over the entire temperature difference range. In contrast, rectification ratios by setting D^H to Ph and Py merged at large ΔT, indicating that the asymmetry between Ph and Py in the diblock was less important for the thermal diode. This contrasts with the case of an electrical diode of the *pn*-resembling diblock molecule presented in Refs. [28, 44], as the electrical properties of molecular elements, are directly related to rectification, while the atomic structure and the mass of the elements play dominant roles in phonon thermal transport.

When the spacer consisted of two HBs, the rectification ratio increased more clearly, as shown by the η of $(CHO_2)_2$**Ph**Ph in Table 2. As stated in Section III, a much larger dephasing effect was observed in $(CHO_2)_2Ph_2$ compared to the other diblock molecules because of the two HBs. These results demonstrated the potential advantage of HB as a spacer, which should include the reciprocity function, i.e., sufficient thermal conductivity and the separation of vibrational modes on D^H and A^H locally. The function of a separator is related to the large dephasing at the spacer as well as the introduced asymmetric anharmonicity. To directly validate the importance of the dephasing effect at the spacer, we further examined the diblock model based on $(CHO_2)_2$**Ph**Ph, where the self-energy terms on the O and H atoms related to HB were changed from Γ_{0O} and Γ_{0H} to $10\Gamma_{0O}$ and $10\Gamma_{0H}$, respectively. The resulting values of $\eta(\Delta T)$ were more than 1.5 times larger than those of η for the original $(CHO_2)_2$**Ph**Ph, e.g., 7.0% ($\Delta T = 300$ K) and 17.7% ($\Delta T = 500$ K). The two HBs were symmetrically located on D^H (Ph) and A^H (Ph). Therefore, we concluded that our inference was reasonable: the anharmonicity built into the spacer promoted the separation of thermal properties of D^H and A^H while maintaining the thermal conductive path between the two moieties.

In the calculations this far, we have fixed the reference temperature T_0 at 100 K and varied ΔT. Thus, the electrode in the low-temperature regime was at 100 K. When a higher reference temperature is adopted, the maximum values of T_A or T_D also become higher than in the case of T_0 = 100 K, and an increase in the rectification function can be expected due to the suppression of heat current by enhanced phonon scatterings in D^H. The values of $\eta(\Delta T)$ for (CHO_2)**Ph**Ph with the reference temperature set to 300 K were almost twice those at 100 K. For example, η was 10.3%, 15.4%, and 21.7% for ΔT = 300, 400, and 500 K, respectively. In Figure 4, the $J_Q - \Delta T$ characteristics, which are analog to *I–V* characteristics, are given for T_0 = 100 and 300 K. The heat current in the forward direction was nearly a linear function; close to that predicted by the ballistic approximation. In contrast, we found strong nonlinearity in the backward current with decreasing ΔT from 0 K, i.e., when a negative temperature bias was applied. This coexistence of linearity and nonlinearity is characteristic of the thermal transport in the present AR-resembling molecular junction. This is different from the AR (or *pn* junction) electric diode, where I–V curves in both forward and backward directions are nonlinear due to tunneling transport and bias-induced level shifts of molecular orbitals.

To illustrate the dephasing effect to rectification more directly, we give a brief consideration based on lowest perturbation theory as well as calculated results. When the lowest order perturbation is applied by expansion of self-energy of *enhanced* anharmonicity, $\Pi^{r/a}_{\mathrm{vib(add)}}$, the elastic transmission coefficient of $(CHO_2)_2$**Ph**Ph, $\overline{\mathcal{T}}^{ela}$, is expressed by that of $(CHO_2)_2Ph_2$, $\mathcal{T}^{ela}$, as follows:

$$\overline{\mathcal{T}}^{ela} = \mathcal{T}^{ela} + 2\mathrm{Tr}\left[\mathrm{Re}\left(\Gamma_L D^r \Pi^r_{\mathrm{vib(add)}} D^r \Gamma_R D^a\right)\right] + o\left((\Pi^r_{\mathrm{vib(add)}})^2\right) \qquad (11)$$

where $D^{r/a}$ is Green's function of $(CHO_2)_2Ph_2$. The second term is usually negative value and relating to dephasing effect by enhanced phonon scatter. Recall that $\Pi^r_{\mathrm{vib(add)}}$ is added to the atomic site of D^H and $\Pi^r_{\mathrm{vib(add)}}$ depends on local temperature of atomic site of D^H side through $\tau_a^{-1}(\omega, T = T_\mu)$. Therefore, magnitude of the second term in Eq. (11) is greater when the D^H side is in higher temperature (negative temperature bias, i.e., backward direction) than when A^H side is in higher temperature (positive temperature bias, i.e., forward direction). We showed calculated $\overline{\mathcal{T}}^{ela}$ of the case of positive $(\Delta T = 500K)$ and negative $(\Delta T = -500K)$ temperature bias in SI.

Though we demonstrated thermal rectification and nonlinearity in our proposed AR-resembling diblock molecular junctions, the enhanced rectification is at most 20%. Two reasons can be considered for such suppression of rectification. The first reason is that the heat current at the interface of D^H and the electrode is assisted by inelastic phonon scattering, as shown in Section III, thereby canceling some of the suppression of thermal transport through high-temperature D^H by the dephasing effect. The second is the screening of the temperature gradient in the diblock molecule. We evaluated the local temperature T_{I_a} of each atom I_a by averaging $T_{\in I_a}$ for the (CHO_2)**Ph**Ph junction and found that the maximum difference in local temperatures between the atoms in D^H and A^H is less than 10% of the given ΔT. Most of the temperature gradient is realized as the temperature drop at the interface, i.e., the Au electrode and linker thiolate atom. This temperature screening effect results from the mismatching of phonon DOS between the electrode and the molecule due to differences in mass and the number of phonons.

Conclusion

In summary, we extended the concept of the AR diode (more strictly, the *pn* junction resembling the diblock molecular diode) to design a single molecular thermal diode. Our design consisted of two ideas: (i) constructing molecular blocks of different anharmonicity by introducing phonon scatterers, i.e. side-chains, asymmetrically, and (ii) using HB as the spacer, which is sufficiently thermally conductive but also acts as a separator. For this purpose, we developed a systematic method of thermal transport calculations, combining classical MD and NEGF to incorporate a nonempirical and more conventional anharmonic self-energy term than strict perturbation theory.

Our calculations demonstrate the usefulness of AR-resembling diblock molecules as a principle for designing molecular thermal devices. In particular, using HBs as functional thermal conductors (spacers) is promising. However, the magnitude of the rectification ratio was not satisfactory for practical uses, similar to the case of electric diodes. Our theoretical analysis highlighted both the limitations and necessary improvements. One possibility is using carbon material as thermal electrodes to avoid phonon mismatching. Then features of molecular internal vibrational modes and their

interactions can be more directly relating to thermal transport. Furthermore, reducing mismatching by hetero junction, inelastic thermal current may be suppressed. As results, one can expect that rectification ration reflects difference of dephasing effect between forward and backward directions directly. Another possibility is introducing a dense and thick AR-resembling molecular film, where D^H and A^H moieties are connected tightly to each side of electrode and separated by HB, as a thermal resistance layer instead of a single molecule to realize a sufficient temperature gradient. Furthermore, it is expected that AR-resembling molecular film increases anharmonicity of HB by two dimensional HB network and that to D^H moieties caused by intermolecular interactions. The former enhances the role of the spacer, and the latter makes more distinct D^H and A^H by introducing side chains.

Data availability

The data and simulation protocols supporting this article have been included as part of ESI.

Conflicts of interest

The authors declare that no conflict of interest in this manuscript.

ACKNOWLEDGMENTS

This work was supported by CREST, JST, Grant No. JPMJCR18I4.

REFERENCES

(1) Kiguchi, M.; Ohto, T.; Fujii, S.; Sugiyasu, K.; Nakajima, S.; Takeuchi, M.; Nakamura, H. Single Molecular Resistive Switch Obtained via Sliding Multiple Anchoring Points and Varying Effective Wire Length. *Journal of the American Chemical Society* **2014**, *136* (20), 7327-7332. DOI: 10.1021/ja413104g.
(2) Sanvito, S. Molecular spintronics. *Chemical Society Reviews* **2011**, *40* (6), 3336-3355. DOI: 10.1039/c1cs15047b.
(3) Kubatkin, S.; Danilov, A.; Hjort, M.; Cornil, J.; Brédas, J. L.; Stuhr-Hansen, N.; Hedegård, P.; Bjornholm, T. Single-electron transistor of a single organic molecule with access to several redox states. *Nature* **2003**, *425* (6959), 698-701. DOI: 10.1038/nature02010.
(4) Zhang, Q.; Sun, Y. M.; Xu, W.; Zhu, D. B. Organic Thermoelectric Materials: Emerging Green Energy Materials Converting Heat to Electricity Directly and Efficiently. *Advanced Materials* **2014**, *26* (40), 6829-6851. DOI: 10.1002/adma.201305371.
(5) Huang, Z. F.; Xu, B. Q.; Chen, Y. C.; Di Ventra, M.; Tao, N. J. Measurement of current-induced local heating in a single molecule junction. *Nano Letters* **2006**, *6* (6), 1240-1244. DOI: 10.1021/nl0608285.
(6) Aradhya, S. V.; Venkataraman, L. Single-molecule junctions beyond electronic transport. *Nature Nanotechnology* **2013**, *8* (6), 399-410. DOI: 10.1038/nnano.2013.91.
(7) Tsutsui, M.; Taniguchi, M. Single Molecule Electronics and Devices. *Sensors* **2012**, *12* (6), 7259-7298. DOI: 10.3390/s120607259.
(8) Pop, E. Energy Dissipation and Transport in Nanoscale Devices. *Nano Research* **2010**, *3* (3), 147-169. DOI: 10.1007/s12274-010-1019-z.
(9) Breuer, H. P.; Laine, E. M.; Piilo, J.; Vacchini, B. Colloquium: Non-Markovian dynamics in open quantum systems. *Reviews of Modern Physics* **2016**, *88* (2). DOI: 10.1103/RevModPhys.88.021002.
(10) Meng, Q. S.; Zhang, J. X.; Zhang, Y.; Chu, W. Z.; Mao, W. J.; Zhang, Y.; Yang, J. L.; Luo, Y.; Dong, Z. C.; Hou, J. G. Local heating and Raman thermometry in a single molecule. *Science Advances* **2024**, *10* (3). DOI: 10.1126/sciadv.adl1015. Chen, H. L.; Jia, C. C.; Zhu, X.; Yang, C.; Guo, X. F.; Stoddart, J. F. Reactions in single-molecule junctions. *Nature Reviews Materials* **2023**, *8* (3), 165-185. DOI: 10.1038/s41578-022-00506-0.
(11) Lee, W.; Kim, K.; Jeong, W.; Zotti, L. A.; Pauly, F.; Cuevas, J. C.; Reddy, P. Heat dissipation in atomic-scale junctions. *Nature* **2013**, *498* (7453), 209-+. DOI: 10.1038/nature12183.
(12) Majumdar, S.; Sierra-Suarez, J. A.; Schiffres, S. N.; Ong, W. L.; Higgs, C. F., 3rd; McGaughey, A. J.; Malen, J. A. Vibrational mismatch of metal leads controls thermal conductance of self-assembled monolayer junctions. *Nano Lett* **2015**, *15* (5), 2985-2991. DOI: 10.1021/nl504844d From NLM PubMed-not-MEDLINE.
(13) Cui, L. J.; Hur, S.; Akbar, Z. A.; Klöckner, J. C.; Jeong, W.; Pauly, F.; Jang, S. Y.; Reddy, P.; Meyhofer, E. Thermal conductance of single-molecule junctions. *Nature* **2019**, *572* (7771), 628-+. DOI: 10.1038/s41586-019-1420-z.
(14) Mosso, N.; Sadeghi, H.; Gemma, A.; Sangtarash, S.; Drechsler, U.; Lambert, C.; Gotsmann, B. Thermal Transport through Single-Molecule Junctions. *Nano Letters* **2019**, *19* (11), 7614-7622. DOI: 10.1021/acs.nanolett.9b02089.
(15) Fujii, S.; Shoji, Y.; Fukushima, T.; Nishino, T. Visualization of Thermal Transport Properties of Self-Assembled Monolayers on Au(111) by Contact and Noncontact Scanning Thermal Microscopy. *Journal of the American Chemical Society* **2021**, *143* (44), 18777-18783. DOI: 10.1021/jacs.1c09757.
(16) Donadio, D.; Galli, G. Temperature Dependence of the Thermal Conductivity of Thin Silicon Nanowires. *Nano Letters* **2010**, *10* (3), 847-851. DOI: 10.1021/nl903268y. Hu, L.; Zhang, L. F.; Hu,

M.; Wang, J. S.; Li, B. W.; Keblinski, P. Phonon interference at self-assembled monolayer interfaces: Molecular dynamics simulations. *Physical Review B* **2010**, *81* (23). DOI: 10.1103/PhysRevB.81.235427.
(17) Carrete, J.; Vermeersch, B.; Katre, A.; van Roekeghem, A.; Wang, T.; Madsen, G. K. H.; Mingo, N. almaBTE: A solver of the space-time dependent Boltzmann transport equation for phonons in structured materials. *Computer Physics Communications* **2017**, *220*, 351-362. DOI: 10.1016/j.cpc.2017.06.023. Cepellotti, A.; Fugallo, G.; Paulatto, L.; Lazzeri, M.; Mauri, F.; Marzari, N. Phonon hydrodynamics in two-dimensional materials. *Nature Communications* **2015**, *6*. DOI: 10.1038/ncomms7400. Barbalinardo, G.; Chen, Z.; Lundgren, N. W.; Donadio, D. Efficient anharmonic lattice dynamics calculations of thermal transport in crystalline and disordered solids. *Journal of Applied Physics* **2020**, *128* (13). DOI: 10.1063/5.0020443.
(18) Asai, Y. Nonequilibrium phonon effects on transport properties through atomic and molecular bridge junctions. *Physical Review B* **2008**, *78* (4). DOI: 10.1103/PhysRevB.78.045434.
(19) Mingo, N. Anharmonic phonon flow through molecular-sized junctions. *Physical Review B* **2006**, *74* (12). DOI: 10.1103/PhysRevB.74.125402.
(20) Luckyanova, M. N.; Mendoza, J.; Lu, H.; Song, B.; Huang, S.; Zhou, J.; Li, M.; Dong, Y.; Zhou, H.; Garlow, J.; et al. Phonon localization in heat conduction. *Science Advances* **2018**, *4* (12). DOI: 10.1126/sciadv.aat9460.
(21) Joshi, A. A.; Majumdar, A. TRANSIENT BALLISTIC AND DIFFUSIVE PHONON HEAT-TRANSPORT IN THIN-FILMS. *Journal of Applied Physics* **1993**, *74* (1), 31-39. DOI: 10.1063/1.354111.
(22) Markussen, T. Phonon interference effects in molecular junctions. *Journal of Chemical Physics* **2013**, *139* (24). DOI: 10.1063/1.4849178.
(23) Maire, J.; Anufriev, R.; Yanagisawa, R.; Ramiere, A.; Volz, S.; Nomura, M. Heat conduction tuning by wave nature of phonons. *Science Advances* **2017**, *3* (8). DOI: 10.1126/sciadv.1700027.
(24) Zhang, Y.; Lv, Q.; Wang, H.; Zhao, S.; Xiong, Q.; Lv, R.; Zhang, X. Simultaneous electrical and thermal rectification in a monolayer lateral heterojunction. *Science* **2022**, *378* (6616), 169-+. DOI: 10.1126/science.abq0883.
(25) Losego, M. D.; Grady, M. E.; Sottos, N. R.; Cahill, D. G.; Braun, P. V. Effects of chemical bonding on heat transport across interfaces. *Nature Materials* **2012**, *11* (6), 502-506. DOI: 10.1038/nmat3303.
(26) Aviram, A.; Ratner, M. A. MOLECULAR RECTIFIERS. *Chemical Physics Letters* **1974**, *29* (2), 277-283. DOI: 10.1016/0009-2614(74)85031-1.
(27) Ellenbogen, J. C.; Love, J. C. Architectures for molecular electronic computers: 1. Logic structures and an adder designed from molecular electronic diodes. *Proceedings of the Ieee* **2000**, *88* (3), 386-426. DOI: 10.1109/5.838115.
(28) Díez-Pérez, I.; Hihath, J.; Lee, Y.; Yu, L. P.; Adamska, L.; Kozhushner, M. A.; Oleynik, II; Tao, N. J. Rectification and stability of a single molecular diode with controlled orientation. *Nature Chemistry* **2009**, *1* (8), 635-641. DOI: 10.1038/nchem.392.
(29) Ma, H.; Tian, Z. T. Significantly High Thermal Rectification in an Asymmetric Polymer Molecule Driven by Diffusive versus Ballistic Transport. *Nano Letters* **2018**, *18* (1), 43-48. DOI: 10.1021/acs.nanolett.7b02867.
(30) Xu, Y.; Wang, J.-S.; Duan, W.; Gu, B.-L.; Li, B. Nonequilibrium Green's function method for phonon-phonon interactions and ballistic-diffusive thermal transport. *Physical Review B* **2008**, *78* (22). DOI: 10.1103/PhysRevB.78.224303. Wang, J. S.; Zeng, N.; Wang, J.; Gan, C. K. Nonequilibrium Green's function method for thermal transport in junctions. *Physical Review E* **2007**, *75* (6). DOI: 10.1103/PhysRevE.75.061128.
(31) Luisier, M. Atomistic modeling of anharmonic phonon-phonon scattering in nanowires. *Physical Review B* **2012**, *86* (24). DOI: 10.1103/PhysRevB.86.245407.

(32) Buttiker, M. ROLE OF QUANTUM COHERENCE IN SERIES RESISTORS. *Physical Review B* **1986**, *33* (5), 3020-3026. DOI: 10.1103/PhysRevB.33.3020.
(33) Anantram, M. P.; Datta, S. Effect of phase breaking on the ac response of mesoscopic systems. *Phys Rev B Condens Matter* **1995**, *51* (12), 7632-7639. DOI: 10.1103/physrevb.51.7632 From NLM PubMed-not-MEDLINE.
(34) Miao, K.; Sadasivam, S.; Charles, J.; Klimeck, G.; Fisher, T. S.; Kubis, T. Büttiker probes for dissipative phonon quantum transport in semiconductor nanostructures. *Applied Physics Letters* **2016**, *108* (11). DOI: 10.1063/1.4944329. Fereidani, R. M.; Segal, D. Phononic heat transport in molecular junctions: Quantum effects and vibrational mismatch. *Journal of Chemical Physics* **2019**, *150* (2). DOI: 10.1063/1.5075620.
(35) Nakamura, H. Thermoelectric and Thermal Properties of a (GeTe)₂/Sb₂Te₃ Interfacial Phase-Change Memory Device. *Physica Status Solidi-Rapid Research Letters* **2021**, *15* (3). DOI: 10.1002/pssr.202000393.
(36) Sääskilahti, K.; Oksanen, J.; Tulkki, J. Thermal balance and quantum heat transport in nanostructures thermalized by local Langevin heat baths. *Physical Review E* **2013**, *88* (1). DOI: 10.1103/PhysRevE.88.012128. Savin, A. V.; Kosevich, Y. A.; Cantarero, A. Semiquantum molecular dynamics simulation of thermal properties and heat transport in low-dimensional nanostructures. *Physical Review B* **2012**, *86* (6). DOI: 10.1103/PhysRevB.86.064305. Wang, J. S. Quantum thermal transport from classical molecular dynamics. *Phys Rev Lett* **2007**, *99* (16), 160601. DOI: 10.1103/PhysRevLett.99.160601 From NLM PubMed-not-MEDLINE.
(37) Daldrop, J. O.; Kappler, J.; Brünig, F. N.; Netz, R. R. Butane dihedral angle dynamics in water is dominated by internal friction. *Proceedings of the National Academy of Sciences of the United States of America* **2018**, *115* (20), 5169-5174. DOI: 10.1073/pnas.1722327115. Gottwald, F.; Karsten, S.; Ivanov, S. D.; Kühn, O. Parametrizing linear generalized Langevin dynamics from explicit molecular dynamics simulations. *Journal of Chemical Physics* **2015**, *142* (24). DOI: 10.1063/1.4922941. Kowalik, B.; Daldrop, J. O.; Kappler, J.; Schulz, J. C. F.; Schlaich, A.; Netz, R. R. Memory-kernel extraction for different molecular solutes in solvents of varying viscosity in confinement. *Physical Review E* **2019**, *100* (1). DOI: 10.1103/PhysRevE.100.012126. Tepper, L.; Dalton, B.; Netz, R. R. Accurate Memory Kernel Extraction from Discretized Time-Series Data. *Journal of Chemical Theory and Computation* **2024**, *20* (8), 3061-3068. DOI: 10.1021/acs.jctc.3c01289.
(38) Maassen, J.; Zahid, F.; Guo, H. Effects of dephasing in molecular transport junctions using atomistic first principles. *Physical Review B* **2009**, *80* (12). DOI: 10.1103/PhysRevB.80.125423.
(39) Nakamura, H.; Yamashita, K.; Rocha, A. R.; Sanvito, S. Efficientab initiomethod for inelastic transport in nanoscale devices: Analysis of inelastic electron tunneling spectroscopy. *Physical Review B* **2008**, *78* (23). DOI: 10.1103/PhysRevB.78.235420.
(40) Rocha, A. R.; García-Suárez, V. M.; Bailey, S.; Lambert, C.; Ferrer, J.; Sanvito, S. Spin and molecular electronics in atomically generated orbital landscapes -: art. no. 085414. *Physical Review B* **2006**, *73* (8). DOI: 10.1103/PhysRevB.73.085414. Rungger, I.; Sanvito, S. Algorithm for the construction of self-energies for electronic transport calculations based on singularity elimination and singular value decomposition. *Physical Review B* **2008**, *78* (3). DOI: 10.1103/PhysRevB.78.035407.
(41) Callaway, J. Model for Lattice Thermal Conductivity at Low Temperatures. *Physical Review* **1959**, *113* (4), 1046-1051. DOI: 10.1103/PhysRev.113.1046.
(42) Sadasivam, S.; Ye, N.; Feser, J. P.; Charles, J.; Miao, K.; Kubis, T.; Fisher, T. S. Thermal transport across metal silicide-silicon interfaces: First-principles calculations and Green's function transport simulations. *Physical Review B* **2017**, *95* (8). DOI: 10.1103/PhysRevB.95.085310.
(43) Gemma, A.; Tabatabaei, F.; Drechsler, U.; Zulji, A.; Dekkiche, H.; Mosso, N.; Niehaus, T.; Bryce, M. R.; Merabia, S.; Gotsmann, B. Full thermoelectric characterization of a single molecule. *Nat*

Commun 2023, *14* (1), 3868. DOI: 10.1038/s41467-023-39368-7 From NLM PubMed-not-MEDLINE.
(44) Nakamura, H.; Asai, Y.; Hihath, J.; Bruot, C.; Tao, N. Switch of Conducting Orbital by Bias-Induced Electronic Contact Asymmetry in a Bipyrimidinyl-biphenyl Diblock Molecule: Mechanism to Achieve a pn Directional Molecular Diode. *The Journal of Physical Chemistry C* 2011, *115* (40), 19931-19938. DOI: 10.1021/jp205723g.

Figures and Figure captions

(a)

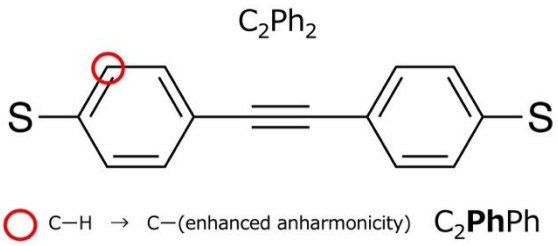

(b)

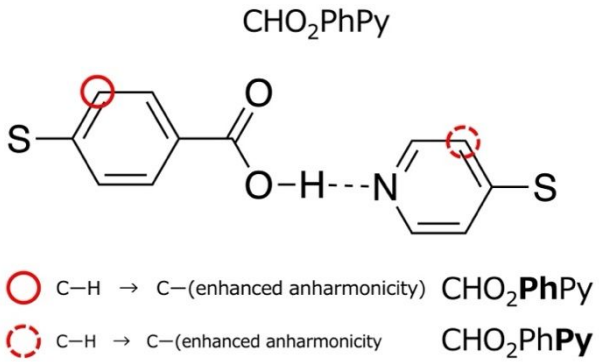

(c)

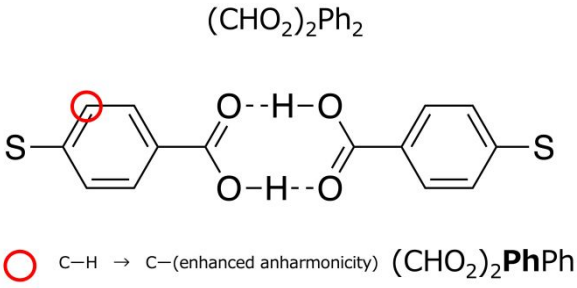

Figure 1. Molecular structure formula of the diblock molecules. Panels (a), (b), and (c) are C_2Ph_2, CHO_2PhPy, and $(CHO_2)_2Ph_2$, respectively. The dot lines represent the hydrogen bonds intended as the spacers. The sites of enhanced anharmonicity to model AR-resembling thermal diode are marked as red circles.

(a)

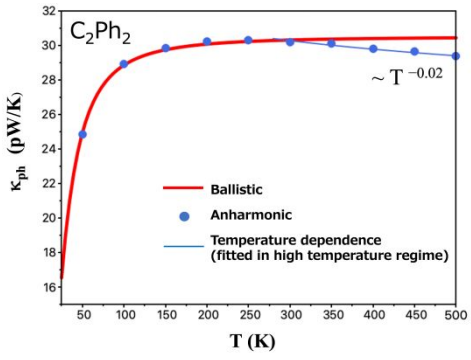

(b)

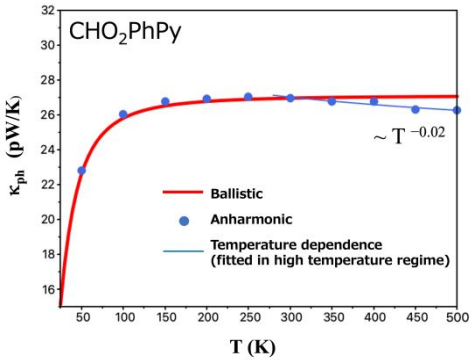

(c)

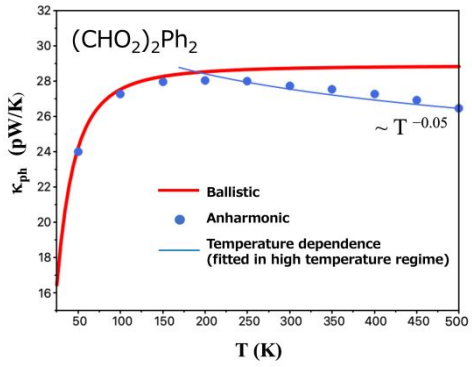

Figure 2. Plots of thermal conductance of (a) C_2Ph_2, (b) CHO_2PhPy, and (c) $(CHO_2)_2Ph_2$ junctions. Red lines are results of ballistic approximation, and blue dots represent the values including anharmonic effects. Thin blue lines extract temperature dependence of thermal conductance as decreasing functions in high temperature regime.

(a) (b)

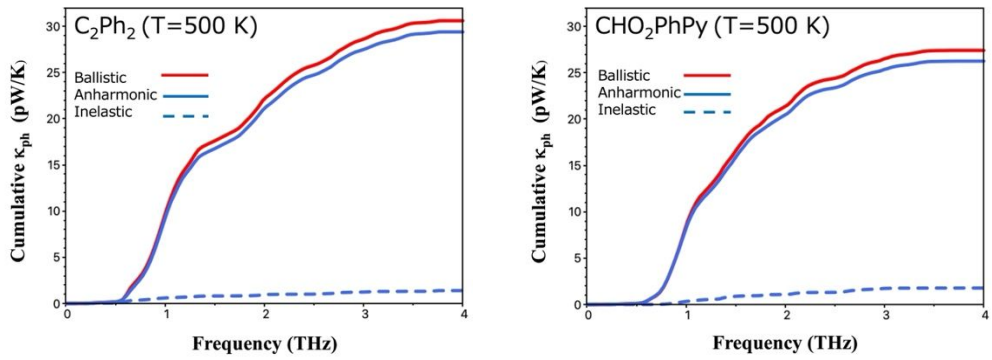

(c)

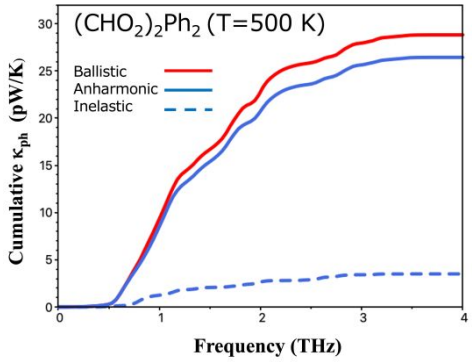

Figure 3. Plots of cumulative thermal conductance as functions of frequency at T = 500K for (a) C_2Ph_2, (b) $(CHO_2)_2PhPy$, and (c) $(CHO_2)_2Ph_2$ junctions, respectively. Blue lines are results including anharmonic effects. The results by ballistic approximation are also plotted by red lines. Blue dot lines represent contribution of inelastic scattering term.

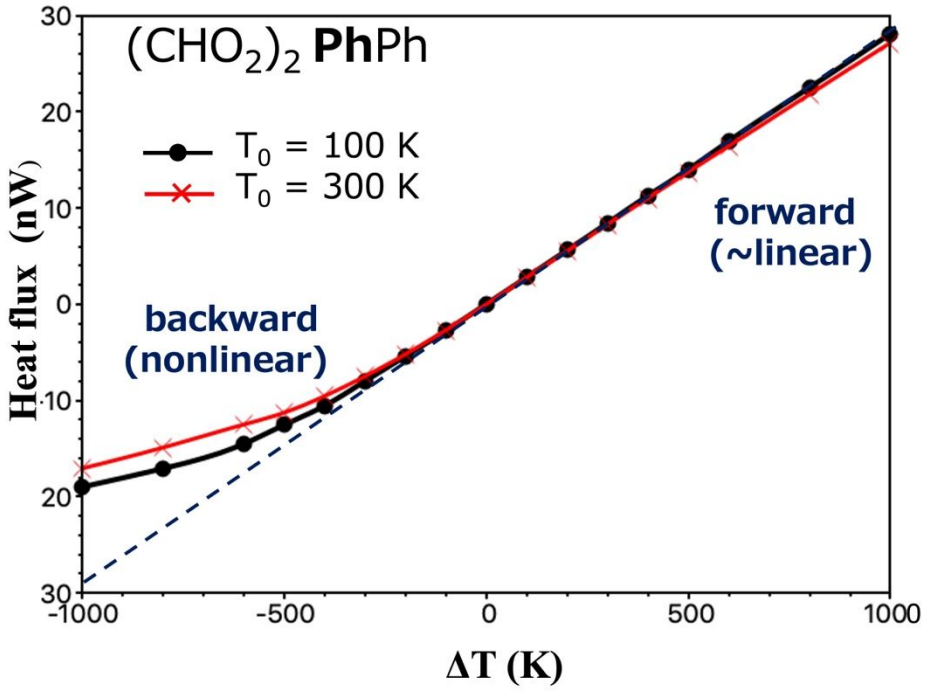

Figure 4. Plots of heat flux as functions of temperature difference ($J_Q - \Delta T$ characteristics) of $(CHO_2)_2$**Ph**Ph junction. Temperature difference is set by reference temperature 100K (black dots and interpolated black line) and 300 K (red cross marks and interpolated red line), respectively.

TABLES

	Γ_0 (s^{-1})	A	α_T (K^{-1})	B	β_T (K^{-1})	α_w (s)
H	1.57×10^{11}	3.14×10^{-2}	8.44×10^{-3}	1.18×10^{-2}	2.92×10^{-3}	5.26×10^{-13}
C	1.56×10^{11}	8.63×10^{-3}	7.67×10^{-3}	9.58×10^{-3}	2.93×10^{-3}	5.92×10^{-13}
N	1.56×10^{11}	2.78×10^{-2}	5.59×10^{-3}	2.90×10^{-3}	2.54×10^{-3}	7.57×10^{-13}
O	1.56×10^{11}	2.78×10^{-2}	5.59×10^{-2}	2.90×10^{-3}	2.54×10^{-3}	7.57×10^{-13}
S	1.56×10^{11}	5.32×10^{-3}	6.66×10^{-3}	3.48×10^{-3}	3.16×10^{-3}	6.18×10^{-13}

Table 1. The friction constant given in Eq. (7) and parameters of the model function of color noise defined by Eq. (8) for each atomic species.

ΔT (K)	η (%)			
	C_2**Ph**Ph	CHO_2**Ph**Py	CHO_2Ph**Py**	$(CHO_2)_2$**Ph**Ph
100	0.5	0.8	0.7	1.2
200	0.7	1.3	1.3	2.4
300	1.0	2.7	4.0	5.2
400	4.2	4.8	6.7	6.7
500	6.2	9.5	9.9	11.6

Table 2. Rectification parameters of the asymmetric anharmonicity-induced molecular junctions for the reference temperature T_0=100K.

Data availability statements

The data and simulation protocols supporting this article have been included as part of ESI.